Electrostatic Deposition of Polyionic Monolayers on Charged Surfaces†

V. V. Tsukruk,*,‡ V. N. Bliznyuk,§ and D. Visser

College of Engineering and Applied Sciences, Western Michigan University, Kalamazoo, Michigan 49008

A. L. Campbell,*,|| T. J. Bunning, and W. W. Adams

Materials Directorate, Wright Laboratory, WL/MLPJ, Building 651, 3005 P Street, Ste 1, Wright-Patterson AFB, Ohio 45433-7702

Received December 26, 1996; Revised Manuscript Received April 16, 1997⊗

ABSTRACT: We explored molecular films of polyionic materials built by electrostatic deposition on a charged surface. Formation of self-assembled monolayers is monitored for poly(styrenesulfonate) (PSS) adsorbed on charged surfaces of amine-terminated self-assembled monolayer (SAM) and poly(allylamine) (PAA) on a PSS monolayer. In both cases, polyions are adsorbed on oppositely-charged surfaces. Observations of PSS monolayers at various stages of electrostatic deposition reveal inhomogeneous self-assembly at the earliest stages of deposition. During the first several minutes of deposition, negatively-charged PSS macromolecules tend to adsorb on selected defect sites of positively-charged SAM (scratches, microparticles, and edges) and form islands composed of PSS coils. At this stage, electrostatic adsorption of PSS chains is predominant and equilibration of the surface structure is not achieved by the slow surface diffusion mechanism. Only longer deposition times (>10 min) result in an equilibration of polymer layers and formation of a homogeneous thin PSS layer composed of highly flattened macromolecular chains. The monolayer thickness is between 1.0 and 1.5 nm, with a microroughness of about 0.2 nm. Self-assembly of a second PAA layer on top of a PSS monolayer follows similar tendencies, resulting in the formation of homogeneous PAA/PSS bilayers with an overall thickness of 1.7−2.5 nm.

Introduction

Currently, several approaches exist for fabrication of organized molecular assemblies from functional macromolecular materials.[1−3] The Langmuir−Blodgett (LB) technique is suitable for the fabrication of organized monolayers from amphiphilic molecules at the air−water interface when transferred onto a solid substrate.[2,3] Chemisorption of molecules with functional terminal groups like alkylsilanes on solid substrates with the "right" surface groups results in the formation of robust uniform self-assembled monolayers (SAMs) chemically tethered to this surface.[1] Finally, electrostatic layer-by-layer deposition exploits Coulombic interactions between oppositely-charged molecules physically adsorbed from dilute solutions in an alternative method.[4] It has been shown that this last approach can be used to build ordered multilayer films (hundreds of layers) with various combinations of molecular fragments, organic and inorganic layers, latexes, molecules with switchable conformation, biomolecules, photochromic molecules, and conductive polymers.[4−10]

The layer-by-layer self-assembling process in its initial stage requires special attention. The mechanical and temporal stability of the first molecular layers tethered to a solid substrate is a critical element to the homogeneity of thicker films. The concentration of interlayer defects depends to a great extent upon the homogeneity, affinity, and microroughness of this first monolayer. A gradient of molecular ordering across the first several (usually 3−5) molecular layers is observed for various molecular films.[2,5,11] This phenomenon is usually related to healing of substrate inhomogeneities and nonequilibrium behavior. Formation of nonequilibrium surface morphologies and inhomogeneous coverage is caused by the competition of the kinetics of polymer chain adsorption and their surface diffusion.

Obviously, kinetic limitations are imposed on the formation of organized multilayers from polyionic materials. In fact, stable and consistent layer-by-layer growth of self-assembled films is observed only after a certain deposition time.[5] It is speculated that assembly of polyions on charged surfaces is indeed a two-stage process: macromolecular chains are anchored to the surface by some segments during the short initial stage and then relax to a dense packing during the long second stage of self-assembly. Presumably, a stable homogeneous polymer monolayer which covers the original surface is formed only after complete "relaxation" of adsorbed macromolecules. These and other singularities are supported by numerous *indirect observations* of layer-by-layer deposition behavior. However, to date, no *direct structural data* exist regarding the actual surface morphology of these first molecular layers at different stages of their growth and their evolution during fabrication of multilayer self-assembled films.

In the present paper, we report direct observations of the formation of the first polyionic monolayer and bilayer during electrostatic deposition of charged amorphous polyions on oppositely-charged surfaces. The negatively−positively-charged polymer pairs of poly(styrenesulfonate) (PSS) and poly(allylamine) (PAA) are selected for this study, and the positively-charged surface is an amine-terminated self-assembled monolayer (SAM) chemisorbed on a silicon wafer (see Figure 1 for a general scheme and chemical formulas).

* To whom correspondence should be addressed.

† Dedicated to Prof. Yu. Lipatov on the occasion of his 70 birthday.

‡ Fax: 616-387-6517. Email: vladimir@wmich.edu.

§ Institute of Semiconductor Physics, Ukrainian Academy of Science, Kiev 252650, Ukraine.

|| Fax: 513-255-1128. Email: campbeal@ml.wpafb.af.mil.

⊗ Abstract published in *Advance ACS Abstracts,* October 1, 1997.

S0024-9297(96)01897-9 CCC: $14.00

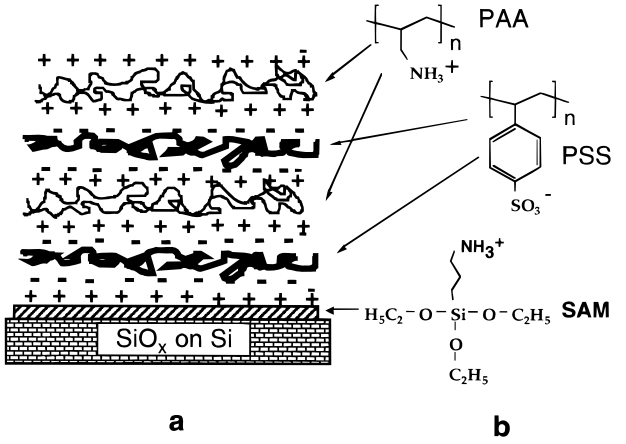

Figure 1. General scheme of multilayer self-assembled films formed by electrostatic layer-by-layer deposition (a) and chemical formulas of compounds used (b).

Polymers selected here are frequently used for electrostatic layer-by-layer deposition, give reliable results, are well-characterized in solution, and have been investigated within multilayer films.[5,12−16] However, some irregularities in the earlier stages of layer deposition are reported by various authors which are related to the complex nature of adsorption and formation of self-assembling layers.[5,13] Consistent growth of perfect multilayer films requires adsorption times longer than 10 min. Preliminary observations of inhomogeneity of the first molecular layers of these polymers have been reported by us very recently.[15]

Experimental Section

Schemes of monomeric units of the PSS (M_n = 70 000) and PAA (M_n = 65 000) polyions (Aldrich) are shown in Figure 1b. An electrostatic layer-by-layer deposition technique was employed for the formation of the films from an aqueous solution at neutral conditions as controlled by Milli-Q water used here (pH = 6.5). No attempts to control or change pH were made. At this pH both polyions possess some net charge as a result of dissociation (PSS; the estimated p*K* for terminal sulfonate groups is in the range 1−2) and protonization (PAA; the expected p*K* for terminal amine groups is in the range 7−8) of side groups.[17] Solid substrates used were silicon wafers ((100) orientation, SAS) and float glass (Aldrich) modified by (3-aminopropyl) triethoxysilane (Figure 1b). Cleaning and modification of the substrates as well as the formation and transfer of the monolayers onto the solid supports were performed using rigorous procedures.[1,8] All films were prepared in a class 100 clean room.

Silanized substrates were protonated in a silicon wafer holder with a water solution of 0.01 N HCl. The 0.01 N HCl was poured into the holder and allowed to react for 2 min. The HCl was then poured out, and the substrates in the holder were flushed under running Milli-Q water. The wafer pieces were then rinsed with Milli-Q water individually and dried with dry nitrogen. The concentrations of the aqueous PSS and PAA solutions were 2 mg/mL, as was determined to be the optimal concentration for fabrication of multilayer films from these polymers.[5] No filtration was used because deposition experiments showed no signs of the presence of foreign particles/aggregates for solutions prepared under class 100 conditions. The protonated substrates were dipped in the PSS solution for the appropriate amount of time as designated below (from 1 s to 64 min). A set of substrates were dipped in the PSS solution for 64 min and were used for the dipping in the PAA solution for different times as designated below. To study kinetics of self-assembly, we used a "freezing" approach. Polyion adsorption was terminated at various periods of time, and specimens were rinsed with Milli-Q water, dried, and studied by scanning probe microscopy, X-ray reflectivity, and ellipsometry.

Atomic force (AFM) and friction force (FFM) images of monolayers in contact and the "tapping" modes were obtained in air at ambient temperature with the Nanoscope IIIA, Dimension 3000 (Digital Instruments, Inc.) according to well-established procedures.[18,19] We observed that a combination of the tapping mode or contact mode scanning with tip modification allowed stable reproducible imaging of the soft monolayers without visible damage. Images were obtained on scales from 200 nm to 100 μm, but for further analysis we selected the two most appropriate "standard" sizes of 2 × 2 μm and 5 × 5 μm. All microroughness values reported here were measured for 1 × 1 μm areas. The AFM tips were modified to introduce appropriate surface charge and avoid tip contamination by charged macromolecules from the specimens (for details see ref 20). Tip radii were in the range 20−40 nm as estimated by scanning a standard specimen with tethered colloidal gold nanoparticles with known diameters according to the published procedure.[21,22] AFM images were obtained for several specimens prepared under identical conditions at different periods of time and at several randomly selected film areas. All structural parameters discussed below were averaged over 7−10 independent measurements.

X-ray reflectivity measurements were performed on a Siemens D-5000 diffractometer equipped with a reflectometry stage. X-ray data were collected within a 0−7° scattering angle range with a step of 0.02° using monochromatized Cu Kα radiation. Measurements within two angle intervals with different parameters (X-ray tube power and accumulation time) were rescaled to one angle interval. Simulation of X-ray curves was done by the REFSIM 1.0 program by direct computation of Fresnel reflectivity.[23] We used standard database densities and refractive indices for the substrates. Polymer film refractive indices were determined from database data for chemical elements in accordance with their chemical composition. For X-ray reflectivity simulations we used a double-layer model of surface structure of silicon substrates (silicon−silicon dioxide layers) with parameters determined independently for bare substrates. For polymer monolayers, we accepted homogeneous density distribution along the surface normal within a single molecular layer with Gaussian interfacial zones.[24] Fitting parameters for polymer films were thickness, specific gravity, and roughness of polymer films.

Ellipsometry measurements were performed with a Rudolph Research Model S2000 thin film ellipsometer and analyzed by using standard values for refractive indices of materials.[25] The thickness of polymer monolayers from ellipsometry was determined by subtracting the thickness of silicon oxide and amine−SAM layers determined for the bare surface of silicon wafers and SAM-coated wafers. Simple molecular models were built by Molecule3D software, and their geometrical sizes were evaluated after energy minimization.

Results and Discussion

Modified Substrates. The surface of silicon wafers is extremely smooth, with no more than 1−2 microscopic defects (holes, bumps, or scratches) per several tens of micron areas. An average root-mean-square (rms) microroughness is 0.2 ± 0.05 nm. The surface of float glass is rougher and contains both surface defects and microscopic waviness, which results in a higher rms roughness of 2.5 ± 1 nm. X-ray reflectivity results confirm these results and show the average macroscopic roughness of 0.4 ± 0.1 nm for silicon wafers and 3 ± 1 nm for glass slides.

Modification of substrate surfaces by chemisorbed SAMs of amine−silane is used to provide the positive surface charges necessary to initiate electrostatic self-assembly of negatively-charged PSS macromolecules. A very light grainy morphology is observed for SAMs which does not disturb the total smoothness of the functional surface. The formation of nanometer-scale domains is typical for SAMs from functional materials and is caused by diffusion-controlled surface segregation

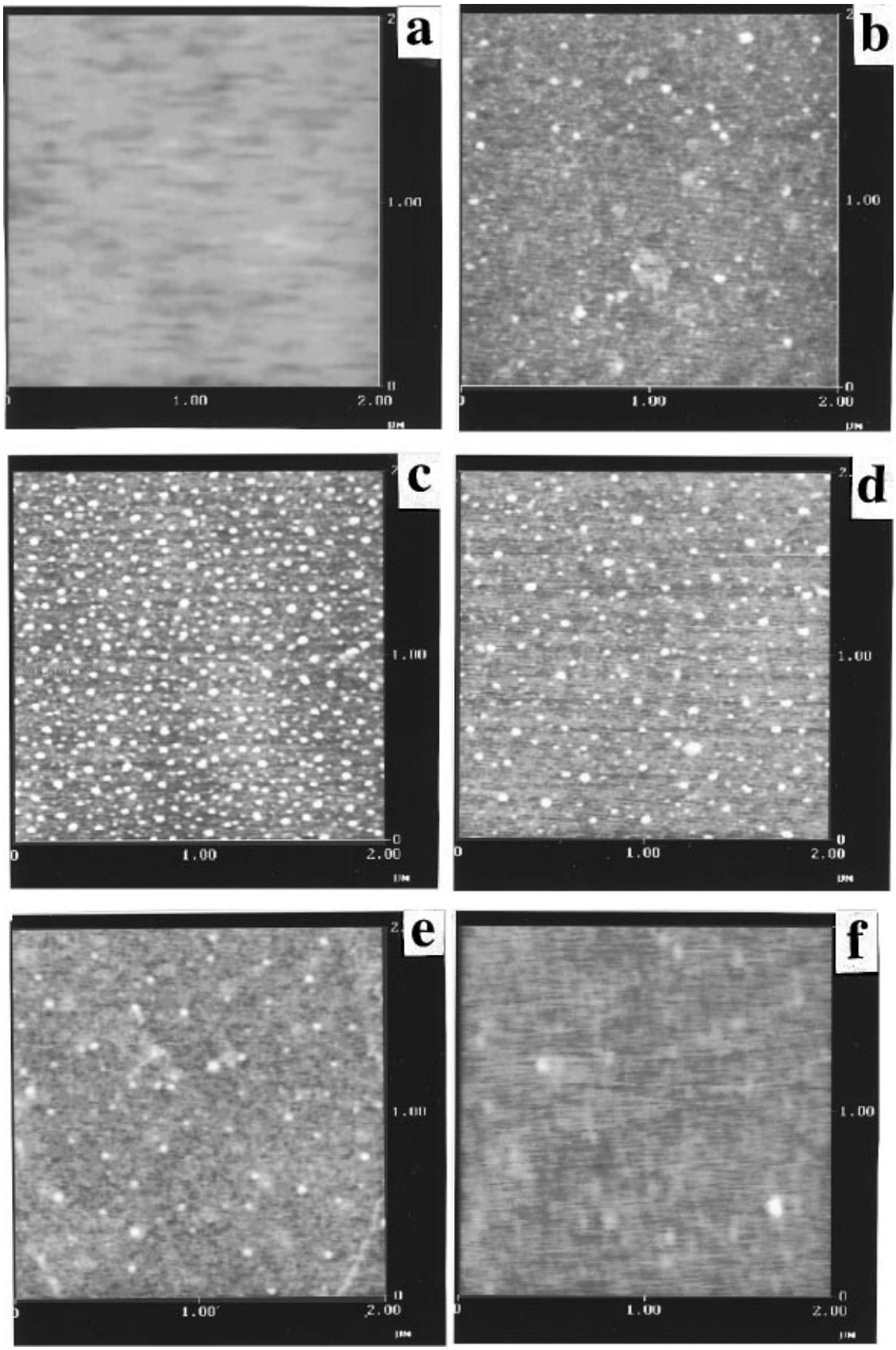

Figure 2. AFM images of a PSS monolayer (2 × 2 μm) at different deposition times: 0 s (amine-terminated SAM) (a), 45 s (b), 2 min (c), 5 min (d), 10 min (e), and 64 min (f).

of monolayer domains, as has been recently demonstrated.[26] This morphology is barely visible on AFM images because of the very small elevations of domains (0.5−0.6 nm) (Figure 2a). As a result, amine−SAMs prepared are very homogeneous, with an average rms microroughness of approximately 0.6 ± 0.2 nm which is close to the silicon surface roughness itself. The thickness of the amine monolayer estimated from occasional holes on the AFM images is about 0.9 ± 0.3 nm, which corresponds closely to the estimated thick-

Table 1. Structural Parameters of Adsorbed PSS Monolayers and a PAA/PSS Bilayer[a]

	height, nm			rms, nm	
time, s	PSS[b]	PSS[c]	PAA[b]	PSS[b]	PAA[b]
0	0	0.0	0	0.23	0.33
10	1.5	1.3		0.17	
20		1.2		2.04	
45	4.0	3.5	1.5	0.17	0.42
120	1.5	2.4	1.4	0.74	
300	1.6	1.7	0.9	0.64	0.32
600	1.0	1.6	1.0	0.16	0.23
1800	2.1	1.2		0.24	
2100			0.7		0.24
3000	1.5	1.2			
3840	1.0	2.0	0.9	0.26	0.22

[a] X-ray thicknesses for the complete PSS monolayer and the complete PAA/PSS bilayer are 1.5 and 2.6 nm, respectively. [b] Data from AFM measurements. [c] Data from ellipsometry.

ness of a monolayer built using amine−silane molecules in an extended conformation (about 1 nm as measured for computer molecular models). The monolayer is very stable and could not be damaged by the AFM tip scanning with high normal loads.

The amine−silane SAMs on the glass surfaces tend to form round domains of a fraction of a micron across. However, the presence of amine−SAM substantially reduces the microroughness of the bare glass substrate to 1.1 ± 0.2 nm, as shown by AFM images (see below). X-ray reflectivity data for modified silicon and glass surfaces confirm these results and give an average thickness of the amine−SAM of 1.3 ± 0.3 nm, fairly close to AFM measurements. The surface of the bare glass and silanized glass is too rough to deduce unambiguous quantitative data for deposited polymer monolayers of several nanometers thickness. Therefore, we make a complete quantitative analysis only for the experimental data obtained on the atomically smooth silicon substrates. General trends observed for glass substrates are discussed as well, but these observations cannot be quantified unambiguously.

PSS Monolayers. The general pattern of surface morphology variation during deposition of PSS molecules for deposition times from 0 s (SAM surface) to 64 min (complete PSS monolayer) is presented in Figure 2. This set of AFM images demonstrates a development of highly heterogeneous morphology in the intermediate stages of monolayer film formation. In the initial stage of PSS self-assembly (less than 5 min) on amine-terminated SAM, the vast majority of the surface remains very smooth (rms roughness is 0.17 nm) (Figure 2b,c and Table 1). Formation of a small amount of isolated islands (<0.3% of surface coverage) is observed in this time interval. The height of isolated islands varied from 1.5 to 4 nm, and their diameter is below 40−50 nm. Most of these islands are randomly distributed over the surface. However, a strong tendency is detected to group in selected places of microscopic surface defects (Figure 3). Figure 3a displays straight rows of islands that are located along submicron scratches and the edges of atomic planes which are occasionally observed for the underlying silicon surface. Sometimes, pieces of PSS monolayers up to several microns across are observed around large-scale defects such as dust particles (Figure 3b). The height of these very smooth pieces of PSS monolayers can be as large as 3.0−4.0 nm.

For longer deposition times (from 2 to 5 min) we observe an increase of surface coverage by randomly distributed islands (Figures 2c,d and 3d). Local coverage increases significantly in the areas of submicron defects such as the edges of atomic planes (Figure 3c). Figure 3d demonstrates the edge of the artificially produced scratch that is used for comparison of underlying silicon surface and polymer layer. Within this time interval, surface microroughness increases substantially and reaches 0.7 nm (Table 1).

A very natural assumption that these islands are composed of adsorbed PSS material and the rest of the surface area represents amine−SAM requires an additional independent confirmation that can be provided by friction force measurements. As is known, FFM mode is highly sensitive to surface chemical composition and allows identification of nonuniformities related to the multicomponent nature of these surfaces.[20,27,28] The difference in friction properties is determined by differences in chemical composition (surface energy and adhesion) and elastic properties (compliance or shear modulus) of the materials probed. FFM images show that frictional properties of underlying surface (amine−SAM) and islands (PSS material) are very different (Figure 4). As can be seen for several islands arranged along the defect line (topographical image in Figure 4a), the friction signal is substantially higher at the tops of the islands than on surrounding areas (Figure 4b). The significant difference in friction responses at identical probing conditions observed for these films (beyond local surface fluctuations and easily recognizable "geometrical effects") indicates the presence of *two different materials* at the surfaces studied. Therefore, at the initial stage we observe PSS material adsorbed in the form of nanometer-sized islands localized around surface defects of the underlying SAM.

In the second stage of adsorption at the longest times tested (10−64 min), the surface of the films possesses a very smooth, homogeneous, slightly grainy topography with a microroughness of 0.25 nm (Table 1 and Figures 2e,f and 5a). Surface chemical composition is *homogeneous*, as indicated by FFM images showing very even friction forces over the film surface (Figure 5b). Therefore, the surface of a complete PSS monolayer at this stage is composed of uniform material. This type of surface morphology is very different as compared to the first stage of PSS adsorption that is marked by highly heterogeneous surface composition. The average thickness of the PSS monolayer decreases to 1 nm for the longest adsorption times (see Table 1). The surface of the complete monolayer becomes very stable and could not be damaged by scanning at higher forces.

X-ray reflectivity curves for incomplete monolayers are very diffuse and produce ambiguous results if interpreted within a homogeneous model approach. However, X-ray reflectivity for complete PSS monolayers shows distinctive features that can be simulated by a double-layer model with a top PSS monolayer of 1.2−1.5 nm thickness (Figure 6). The average density of the PSS layer deduced from simulations is about 1.2 g/cm^3, which indicates a homogeneous and complete monolayer. The macroscopic roughness of these films derived from X-ray simulations is 1.0 ± 0.2 nm.

Ellipsometry measurements for PSS film thicknesses correlate with the variation of surface microstructure observed by AFM on the micron scale (Table 1). We measured the thickness of the silicon oxide layer at 2.5 nm and the thickness of amine−SAM at 0.7 nm, giving a total thickness of the underlying layer of 3.2 nm. The

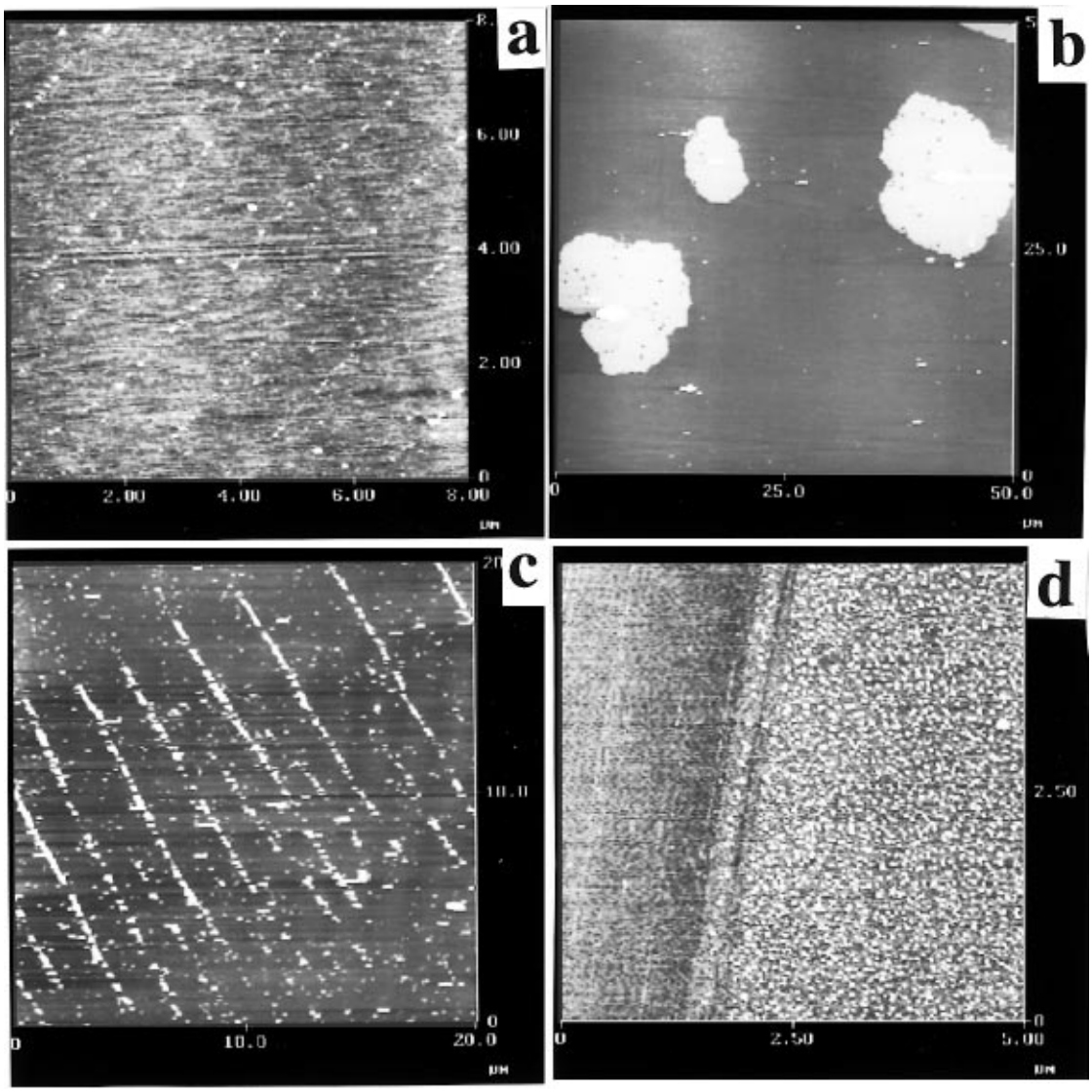

Figure 3. PSS islands formed by electrostatic self-assembly at the shortest deposition times (≈1 min) on surface defects of positively-charged SAM along natural scratches (8 × 8 μm image) (a) and around microparticles (50 × 50 μm image) (b) and at 5 min along the natural scratches (20 × 20 μm) (c) and along the scratch produced by a sharp needle (5 × 5 μm) (d).

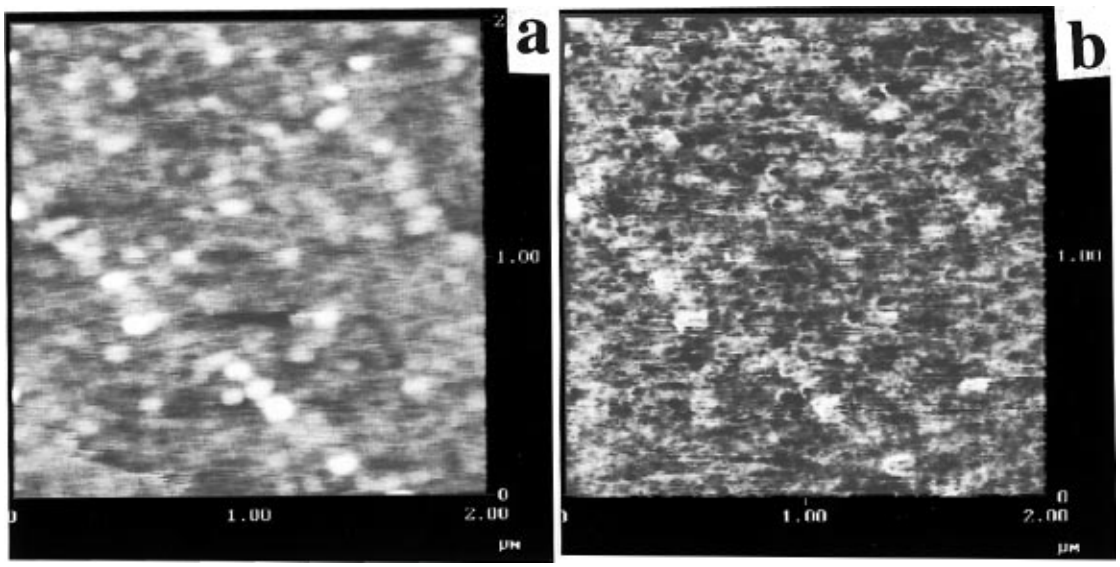

Figure 4. AFM (a) and FFM (b) images of PSS adsorbed at SAM in the initial stages of self-assembly (2 min).

values for sublayers are slightly different as compared to X-ray reflectivity data. However, the overall thickness of 3.2 nm agrees well with the X-ray reflectivity estimation of a total thickness of 2.8 nm (Table 1). Different properties probed (density for X-ray and refractive index for light) as well as variations of

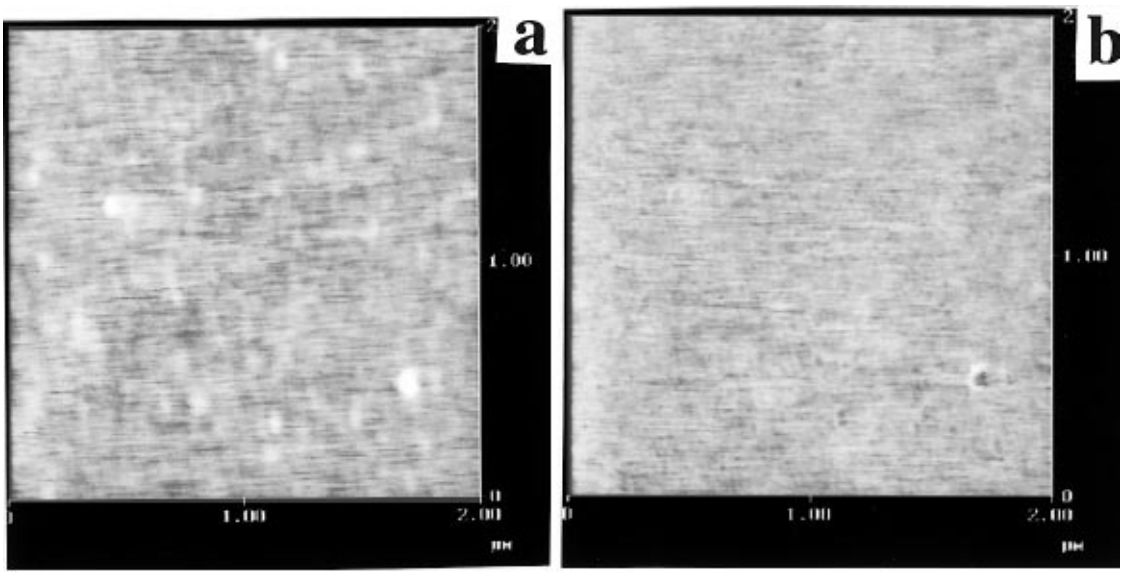

Figure 5. AFM (a) and FFM (b) images of PSS adsorbed at SAM in the latest stages of self-assembly (64 min).

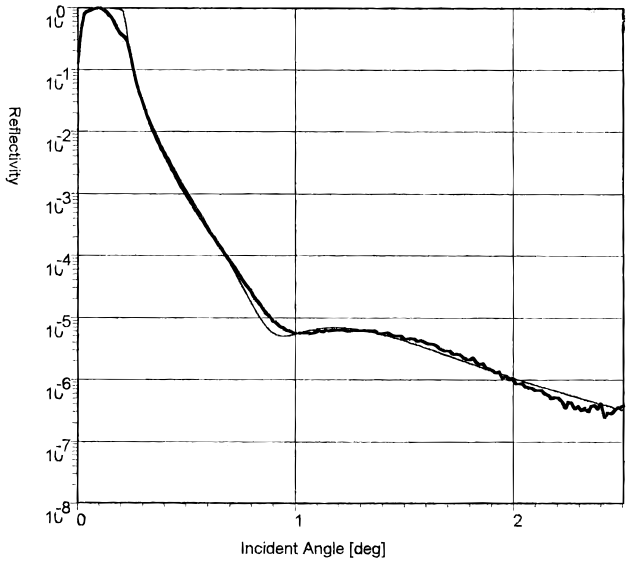

Figure 6. X-ray reflectivity data for a complete PSS monolayer (thick line) and simulated reflectivity for a film with a thickness of 1.5 nm (thin line).

thicknesses from wafer to wafer and for various silanizations can play a role in differences observed.

The total average thickness of the surface layer (silicon oxide + SAM + polymer layer) determined from ellipsometry varies in the range of 4.4−6.7 nm for various deposition times, with a maximum value reached between 1 and 2 min of deposition time. For an estimation of the expected thickness of PSS films we use a simple linear approximation, taking into account that the refractive index for different sublayers is very close (within 1.4−1.5). With these assumptions we obtained reasonably good agreement between AFM and ellipsometry data regarding the variation of PSS monolayer thickness (Table 1). The greatest thickness of the PSS film according to ellipsometry data is in the range 2.4−3.5 nm at the initial fast stage of adsorption.

Generally, time variation of surface morphology during self-assembly of PSS on oppositely-charged glass substrates is similar to that discussed above for silicon wafer surfaces. In this case, the maximum microroughness of about 5 nm is observed at 5 min of adsorption time. Figure 7 shows an example of surface morphology

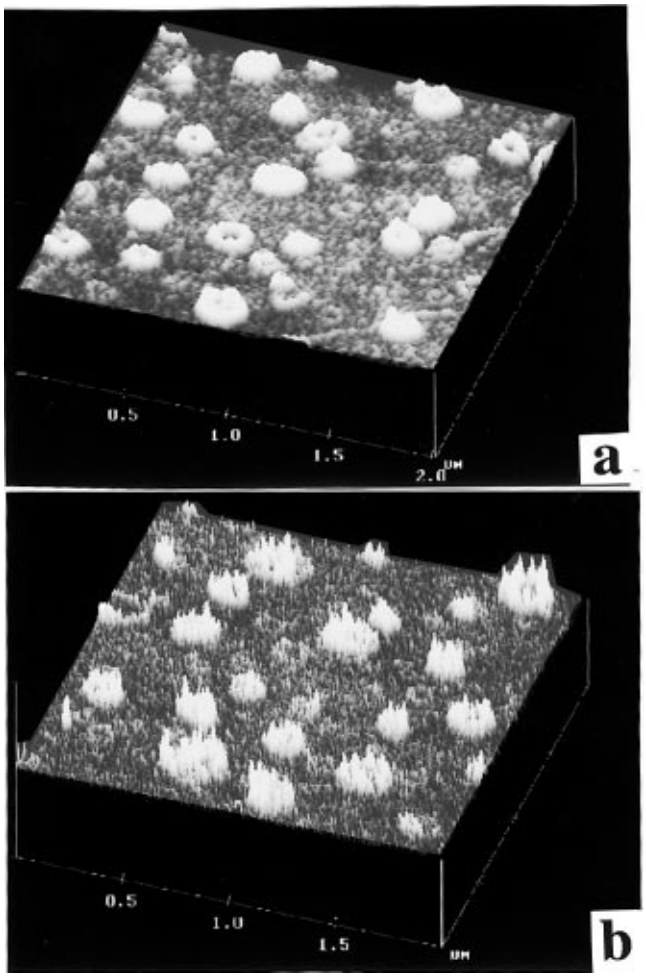

Figure 7. AFM images of a silanized glass surface (a) and the same surface after 2 min of PSS adsorption (b).

of a bare silanized glass (Figure 7a) in comparison with the same substrate after 5 min of PSS deposition (Figure 7b). As can be seen, islands of adsorbed PSS material are concentrated predominantly along the edges of round defect areas in the underlying SAM. This image illustrates how a high concentration of surface morphological features for silanized glass makes it difficult to determine reliable quantitative parameters for adsorbed polymeric material. On the other hand, these results

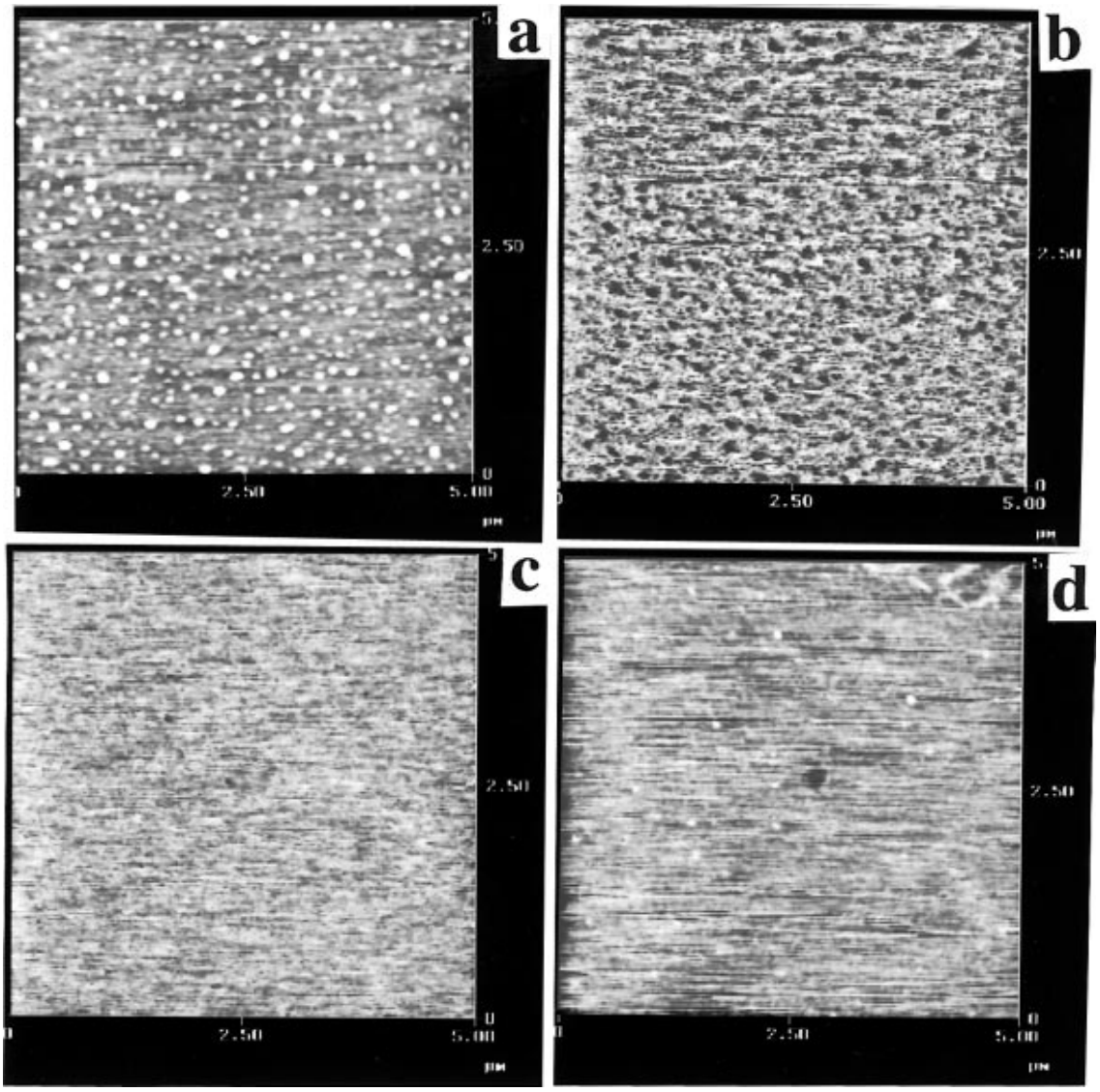

Figure 8. AFM (a, c, d) and FFM (b) images of PAA adsorbed at PSS monolayer in the initial (a, b, 2 min) and the final (c, 34 min; d, 64 min) stages of self-assembly.

confirm a general tendency of PSS macromolecules to adsorb selectively during the first stages of deposition along the surface corrugations and defects.

PSS/PAA Bilayer. General tendencies of the PAA adsorption on an oppositely-charged complete film of PSS are similar to those discussed above. Three major features of the PAA layer formation will be briefly mentioned here.

First, the formation of a complete PAA film takes place much faster, thereby reaching the stage with maximum roughness and randomly distributed islands of PAA materials within the first 2 min (Figure 8a). The presence of the PAA material on top of the PSS layer can be easily recognized by contrast variation in the friction mode, as demonstrated in Figure 8b. The average thickness of the PAA film at this intermediate stage of self-assembly is about 1.2−1.5 nm.

Second, an increase of microroughness at the intermediate stage is significantly more pronounced, as indicated by roughness which reaches 2−3 nm (Table 1). However, complete PAA/PSS bilayers formed at the longest adsorption times are very smooth and possess a very uniform distribution of material (Figure 8c,d). The microroughness (determined from AFM) is in the range 0.2−0.3 nm and the macroroughness (estimated from X-ray reflectivity) is in the range 0.8−0.9 nm for a complete PAA/PSS bilayer (Table 1).

Third, the PAA monolayer assembled on the PSS layer is slightly less stable at intermediate stages of deposition than the PSS film itself. Unlike the PSS layer on SAM, a partially complete PAA film can be damaged by scanning at the highest normal loads. However, the stability of the PAA monolayer increases dramatically at the final stages of self-assembly. The complete PAA film is slightly thinner than the underlying PSS film. The thickness of the complete PAA monolayer determined from AFM is in the range 0.7−0.9 nm (Table 1). X-ray data confirm this difference and give an average PAA layer thickness of 1.1 nm as compared to 1.5 nm for the PSS layer.

Microstructure Models. First of all, our results indicate that models of steady surface adsorption and formation of films by either diffusion-limited or kinetic mechanisms should be considered during the early stages of polyionic monolayer formation because the process of initial deposition of polyionic materials on actual surfaces is substantially inhomogeneous.

Several experimental results reported in the literature indicate a complex character of the surface adsorption of polymers which have specific interactions with

the surfaces (e.g., hydrogen or Coulombic) as compared to low molar mass species. These results are used as a basis for separation of the first (fast) and second (slow) stages of polyion adsorption, as an establishment of a lower time limit for deposition of complete monolayers and consistent growth of multilayer films, and as an explanation of "bimodal" distribution of macromolecular conformations.[5,13,29] The authors reasonably argue that macromolecular chains may deposit more quickly than the surface structure can equilibrate. As a result, a specific bimodal surface structure may be formed with coexisting flattened chains and partially tethered chains with a center of mass above the surface. In addition to this nonequilibrium surface behavior, inhomogeneous adsorption of macromolecules on selected sites such as surface defects and local inhomogeneities in the charge distribution presumably play a decisive role in the surface film formation in the initial stage. However, absence of direct observations of surface microstructure and morphology at the earliest stages of adsorption did not allow confirmation of these speculations. Interestingly enough, the authors who argue nonhomogeneous adsorption use "structure-sensitive" techniques to observe these features. On the other hand, conventional kinetic measurements based on monitoring of macroscopic parameters (e.g., amount of adsorbed material) usually show a monotonic kinetic behavior.

Two main scenarios of epitaxial growth can take place for low molecular mass compounds depending on the surface free energy of the substrate and film and the interface free energy.[30] The first possibility is a Stranski−Krastanov (SK) mode, i.e., initial two-dimensional (2D) layer-by-layer nucleation and growth followed by a transformation toward an agglomerated morphology (2D to 3D transition). The second, Volmer−Weber (VW) mode, is immediate nucleation of three-dimensional islands. In the latter case, complete coverage of the surface will be achieved in subsequent stages of the epitaxy due to further growth and aggregation of these islands. In our case, we have a different growth mechanism that has not been mentioned before. This process possesses specific polymeric features such as the island-type nucleation followed by smearing and thinning of the islands to allow formation of complete coverage. Apparently, smearing of polymer islands includes conformational changes of already adsorbed macromolecules rather than adsorption of new ones (3D to 2D transition). A detailed discussion of this behavior follows.

A model of the film formation by adsorption of charged polyionic macromolecules on an oppositely-charged surface should be based on analysis of all the parameters of surface microstructure described above. A summary of the major parameters of self-assembling PSS and PAA molecular layers versus deposition time, t (heights of domains, H, "ellipsometric" thickness, d_e, microroughnesses, rms) for selected representative specimens is given in Table 1 for both PSS and PAA films and shown graphically in Figure 9. The model discussed below (Figure 10) describes reasonably well the major experimental features observed and requires some rethinking of classical "homogeneous" approaches usually adopted in the field.

At the very initial stage of film formation, within the first 1−2 min of self-assembly, charged PSS polymer chains are adsorbed inhomogeneously, mainly on selected sites of oppositely-charged SAM with high concentrations of local charges (scratches, holes, edges, and foreign microparticles) (Figure 10). At these sites, PSS chains form islands up to 4 nm high, which is close to the geometrical size of macromolecular chains as estimated from molecular weight and the Kuhn segment.[17]

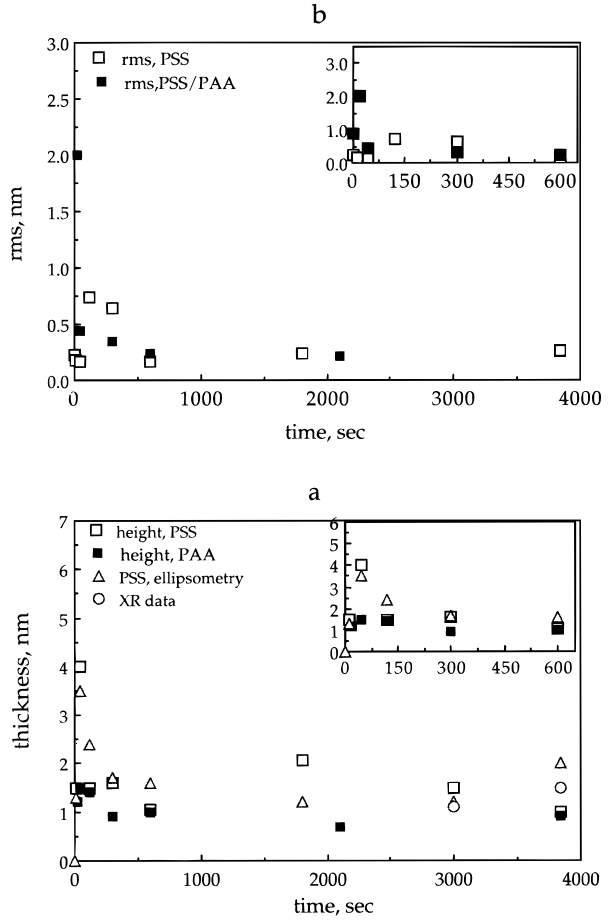

Figure 9. Variation of structural parameters of PSS monolayers: domain heights for PSS and PAA monolayers, thickness of a PSS film from ellipsometry and X-ray reflectivity (a), and microroughness of PSS and PAA monolayers (b) (inserts show earlier time intervals).

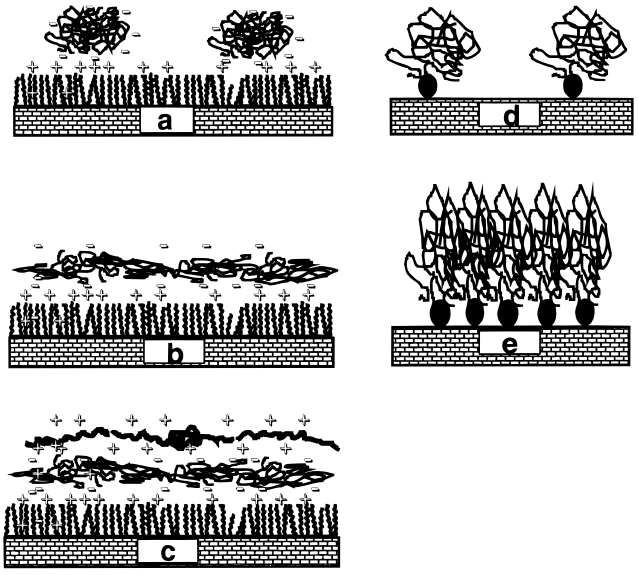

Figure 10. Models of surface microstructure for the polyionic molecular layers: (a) PSS at the shortest deposition time (<5 min); (b) PSS at the longest deposition time (>10 min); (c) PSS/PAA complete bilayer; (d) comparison with polymer brushes in the initial stage of tethering by one sticky end; (e) polymer brushes in a dense state.

Apparently at this stage of deposition, chains are tethered to the surface by only a few segments and thus virtually preserve their coiled conformation. From the estimated average volume of polymer islands at this stage of about 1000 nm^3 (after excluding the tip effect on lateral dimensions[21]), we can conclude that a single island is composed of not more than 10−20 polymer chains. The maximum concentration of isolated islands is observed after 2 min of deposition, resulting in the highest level of microroughness (rms is 0.75 nm) (Figure 9). The limited surface mobility does not allow these chains to spread over the charged SAM during this short time interval.

A longer deposition time allows the PSS surface structure to equilibrate and form a smooth monolayer. Polymer islands are spread out over the surface: their diameters gradually increase to more than 50 nm and their thicknesses decrease to 1−1.5 nm after 30 min (Table 1 and Figure 10). Finally, this results in homogeneous coverage of the surface with flattened PSS chains. These chains form a very thin molecular layer with a thickness of about 2−3 average cross sections of polymer segments. Moreover, this thickness can correspond to just one macromolecular chain if one assumes its organized vertical packing with side groups oriented toward and away from the surface in an alternating manner (Figure 10). The average thickness of a complete PSS monolayer is significantly lower than the equilibrium thickness of a PSS layer in multilayer films. For similar PSS chains within multilayer films the average layer thickness was about 3.4 nm, as observed by neutron reflectivity.[12] Neutron reflectivity provides a unique opportunity for *direct* observation of Bragg reflection from an internal layer structure, unlike X-ray data which give "average" data for total film thickness and cannot resolve multilayer organization due to very smooth density variation along the surface normal.[5] Therefore, we use results on monolayer thickness from ref 12 to compare with our data.

A similar deposition pattern is observed for the formation of a positively-charged PAA monolayer deposited on a completely spread PSS layer (Table 1). The thickness of a complete PAA monolayer is smaller (0.7−1.1 nm) and corresponds to 1−2 cross sections of polymer segments. This value is much smaller than the average thickness of 1.9 nm observed for multilayer films as well by neutron reflectivity.[12]

A high level of spreading in the first molecular layers formed by charged PSS and PAA macromolecules and their fast heterogeneous adsorption might be caused by two major microstructural phenomena. First, a high level of the surface charge for the supporting amine monolayer is present. For a typical packing density within a SAM, one can expect 4−5 charged groups/nm^2 after activation, which is much higher than many "natural" surfaces like mica or silicon (about 2 charged groups/nm^2 at similar conditions).[5,31] Therefore, much higher Coulombic interactions exist in our systems that should accelerate macromolecular adsorption especially at first stages where a number of highly attractive sites exist. Actually, recent AFM studies of PAA adsorption on a weakly-charged mica surface show similar trends but on a much larger time scale: maximum roughness was observed after several hours of adsorption.[32] Second, PSS/PAA macromolecular chains at a given ionic strength of a solution bear substantial ionic charges and thereby must adopt expanded conformation that favors their spreading after adsorption. In fact, it has been demonstrated that partial neutralization of ionic groups in macromolecular chains leads to increased thickness of the adsorbed polyionic layer.[5] It is clear that the ionic state of the macromolecules affects the adsorption mechanism and conformational state of macromolecules tethered to the charged substrate. Accordingly, a variation of polyion concentration in solution may result in a different scenario of polymer adsorption possessing modified kinetic behavior. One can imagine that a higher polyion concentration will increase the probability of fast adsorption of macromolecules at the first stages and, therefore, will affect the following spreading behavior of the macromolecular chains. Obviously, additional observations of surface microstructures at different pHs and solution concentrations are required to completely understand their effects.

Generally, observed variations of surface morphology during the deposition of polyions are completely consistent with multiple reports of the two stages (fast and slow) of polyionic adsorption based on various indirect measurements.[5] The proposed model details structural reorganization of adsorbed macromolecular chains and treats directly these two stages as fast adsorption of macromolecular chains on isolated sites of heterogeneous surfaces in the first stage and their attachment to a surface by a few segments and slow spreading, flattening, and adsorption of macromolecules on a screened surface ("relaxation") during the second slow stage. From a phenomenological point of view, the two-stage kinetic process is similar to that observed and theoretically predicted for the adsorption of macromolecular chains with only one "sticky" end.[33−36]

According to these results, an initial rapid increase of surface coverage is followed by a very slow stage due to the adsorption barrier created by tethered chains. This barrier is caused by an increase in stretching energy due to growing tethering density and the limited space for chain packing and polymer brush formation (macromolecular chains are stretched along the surface normal) (Figure 10). Significant roughening of the polymer layer at specific conditions can be observed for intermediate stages of polymer brush layer formation.[37] Obviously, oppositely-charged polymer chains adsorbed in the fast initial stage play the role of the barrier that slows polyion adsorption during the second stage and screens the Coulombic attraction of the charged surface. However, unlike polymer brushes with one end, multiple sticky sites steer initially adsorbed coiled chains to a very different structural organization (Figure 10). Instead of stretching along the surface normal, the chains are spread and flattened within the surface plane in efforts to reach the maximum concentration of ionic group−surface site contacts.

Another valuable comparison can be done with the interfacial behavior of charged dendritic macromolecules.[38] The results of microstructural studies of dendrimer adsorption at solid surfaces show a *highly compressed* state of dendrimers within compact monolayers. Dendritic macromolecules within molecular layers adopt oblate shape with the axial ratio of 1:3 to 1:5 for various generations. A tendency to higher spreading of high-generation dendrimers observed experimentally corresponds to surface behavior predicted by molecular dynamic simulations for intermediate interaction strengths between sticky groups.[39] Strong interactions between oppositely-charged groups of dendritic macromolecules from adjacent molecular layers (such as ionic binding) are considered to be responsible

for *collapse and compression* of soft trace architecture of dendritic macromolecules within self-assembled films as predicted by molecular computer modeling.[39]

A major limitation of classical models of adsorption as applied to actual charged polymer systems is the assumption of homogeneous and equilibrium molecular adsorption with preservation of the initial state of molecular species (e.g., conformation, orientation).[40−43] This is not true in the case of adsorption of charged *macromolecular* chains on real inhomogeneous surfaces accelerated by strong long-range Coulombic attraction. Apparently, several major features like the defect nature of real surfaces, nonequilibrium adsorption, diffusion behavior, and conformational flexibility play a critical role in the surface behavior observed for polyions and must be taken into full consideration. Probably, the influence of the heterogeneity of the adsorbed surface on the adsorption isotherm can be treated in accordance with the statistical mechanical approach developed for gas adsorption.[40,44] From this consideration, lateral inhomogeneity of the underlying surface favors adsorption at low pressures where the more active sites are empty. However, a significant decrease of surface coverage should be observed for higher pressures. We can speculate that the given conditions of the dilute solution can be similar to low pressure in this theoretical treatment and, therefore, the observed behavior is a reflection of accelerated adsorption onto the heterogeneous surface. Apparently, further development of appropriate theories is required for a complete understanding of the role of surface heterogeneities on electrostatic adsorption of charged macromolecules.

Conclusions

A model of the film formation from charged polyionic PSS and PAA macromolecules adsorbing onto oppositely-charged surfaces has been proposed. This model is based on direct structural observations of the surface morphology variation at different adsorption time intervals. This model specifies two very different stages of surface microstructural variations. At the very initial stage of film formation, within the first 1−2 min of self-assembly, polymer chains are adsorbed *inhomogeneously on selected sites* of the oppositely-charged SAM sublayer with a high concentration of local charges (scratches, holes, edges, and foreign microparticles). At this stage of deposition the chains are tethered to the surface by a few segments only and thus preserve their coiled conformation. Limited surface mobility does not allow them to spread over the charged SAM during this short adsorption time interval.

A longer deposition time allows macromolecules to equilibrate and form a complete monolayer. Polymer islands are gradually spread out over the surface: their height decreases to 1−1.5 nm for adsorption times after 10−30 min. This process results in homogeneous coverage of the surface with flattened macromolecular chains. The chains form a very thin molecular layer with a thickness of not more than 2−3 molecular cross sections, which is significantly lower than the equilibrium thicknesses of PSS and PAA molecular layers within multilayer self-assembled films (2−4 nm). Apparently, the formation of the homogeneous monolayer which completely covers the original surface and causes its recharging is required for consistent growth of multilayer films.

Smaller thicknesses of the first polymer layers might be caused by the high charge density of the substrate surfaces combined with the high concentration of charges for macromolecular chains. Apparently, the high concentration of charges for macromolecular chains (one charged group per each monomeric unit) is sufficient to compensate initial surface charges and recharge the surface. No additional polymer materials are required to "deposit" on the surface. This situation is quite different from the one usually observed for adsorption of weak polyelectrolytes, where high surface charges result in a higher amount of adsorbed polymer.[40,45]

Probably, a variation of ionic strength during the self-assembly process should be considered to keep a uniform thickness of polymer monolayers during the initial stages of the formation of self-assembled films. Finally, selective adsorption of various macromolecular fractions for polydisperse polyions is an important factor in the formation of an inhomogeneous gradient of structural organization at polymer interfaces.[46−48]

Acknowledgment. This work is supported by U.S. Air Force Office for Scientific Research Contract F49620-93-C-0063, U.S. Air Force Contract F33615-95-C-5423, and The Surface Engineering and Tribology Program, The National Science Foundation Grant CMS-94-09431. V.V.T. thanks Humboldt Foundation for support of his summer work at Marburg University and Prof. J. H. Wendorff for X-ray facilities provided. We thank R. F. Lupardo (SAS) for silicon wafers donated and J. Wu for the AFM tip modifications.

References and Notes

(1) Ulman, A. *Introduction to Ultrathin Organic Films*; Academic Press: San Diego, 1991.
(2) Tredgold, R. *Order in Thin Organic Films*; Cambridge University Press: Cambridge, U.K., 1994.
(3) Roberts, G. *Adv. Phys.* **1985**, *34*, 475.
(4) Iler, R. K. *J. Colloid Interface Sci.* **1966**, *21*, 569.
(5) Lvov, Yu. M.; Decher, G. *Crystallogr. Rep.* **1994**, *39*, 628.
(6) Tsukruk, V. V. *Prog. Polym. Sci.* **1997**, *22*, 247. Tsukruk, V. V.; Wendorff, J. H. *Trends Polym. Sci.* **1995**, *3*, 82.
(7) Fendler, H.; Meldrum, F. C. *Adv. Mater.* **1995**, *7*, 607.
(8) Cooper, T. M.; Campbell, A. L.; Crane, R. L. *Langmuir* **1995**, *11*, 2713. Tsukruk, V. V.; Bliznyuk, V. N.; Rinderspacher, F. *Polym. Prepr. (Am. Chem. Soc., Div. Polym. Chem.)* **1996**, *37* (2), 571. Bliznyuk, V. N.; Tsukruk, V. V. *Polym. Prepr. (Am. Chem. Soc., Div. Polym. Chem.)* **1997**, *38* (1), 963.
(9) Ferreira, J. H.; Cheung, M.; Rubner, M. *Thin Solid Films* **1994**, *244*, 806.
(10) Watanabe, S.; Regen, S. L. *J. Am. Chem. Soc.* **1994**, *116*, 8855. Lvov, Yu.; Ariga, K.; Kunitake, T. *Chem. Lett.* **1994**, 2323.
(11) Tsukruk, V. V.; Janietz, D. *Langmuir* **1996**, *12*, 2825.
(12) Schmitt, T.; Grunewald, T.; Decher, G.; Pershan, P.; Kjaer, K.; Losche, M. *Macromolecules* **1993**, *26*, 7058.
(13) Miyano, K.; Asano, K.; Shimomura, M. *Langmuir* **1991**, *7*, 444.
(14) Takahara, A.; Morotomi, N.; Hiraoka, S.; Higashi, N.; Kunitake, T.; Kaliyama, T. *Macromolecules* **1989**, *22*, 617.
(15) Kim, M. W.; Peiffer, D. G. *J. Chem. Phys.* **1985**, *83*, 4159. Bliznyuk, V. N.; Visser, D. W.; Tsukruk, V. V.; Campbell, A. L.; Bunning, T.; Adams, W. *Polym. Prepr.* **1996**, *37* (2), 608.
(16) Maarel, J. R. C.; Groot, L. C.; Hoolander, J. G.; Jesse, W.; Kuil, M. E.; Leyte, J. C.; Leyte-Zuiderweg, L. H.; Mandel, M.; Cotton, J. P.; Jannink, G.; Lapp, A.; Farago, B. *Macromolecules* **1993**, *26*, 7295.
(17) *Handbook of Chemistry and Physics*; Lide, D. R., Ed.; CRC Press: New York, 1996.
(18) Frommer, L. *Angew. Chem., Int. Ed. Engl.* **1992**, *31*, 1298. Tsukruk, V. V.; Reneker, D. H. *Polymer* **1995**, *36*, 1791. Tsukruk, V. V. *Rubber Chem. Technol.* **1997**, accepted for publication.
(19) Tsukruk, V. V., Ratner, B., Eds. *Scanning Probe Microscopy in Polymers;* ACS Symposium Series; American Chemical Society: Washington, DC, 1997, in press.
(20) Tsukruk, V. V.; Bliznyuk, V. N.; Wu, J.; Visser, D. W. *Polym. Prepr. (Am. Chem. Soc., Div. Polym. Chem.)* **1996**, *37* (2), 575. Tsukruk, V. V.; Bliznyuk, V. N. *Langmuir* **1997**, submitted.

(21) Vesenka, J.; Manne, S.; Giberson, R.; Marsh, T.; Henderson, E. *Biophys. J.* **1993**, *65* (9), 992.
(22) Bliznyuk, V. N.; Hazel, J.; Wu, J.; Tsukruk, V. V. In *Scanning Probe Microscopy in Polymers*; Tsukruk, V. V., Ratner, B., Eds.; ACS Symposium Series; American Chemical Society: Washington, DC, 1997, in press.
(23) REFSIM 1.0, Siemens AG, Karlsruhe 7500, Germany, 1994.
(24) Tidswell, J. M.; Rabedeau, T. A.; Pershan, P.; Folkers, J. P.; Baker, M. V.; Whitesides, G. M. *Phys. Rev.* **1991**, *B44*, 10869. Foster, M. *Crit. Rev. Anal. Chem.* **1993**, *24*, 179. Russell, T. P. *Mater. Sci. Rep.* **1990**, *5*, 171. Tsukruk, V. V.; Shilov, V. V. *Structure of Polymeric Liquid Crystals*; Naukova Dumka: Kiev, Ukraine, 1990.
(25) Archer, R. J. In *Ellipsometry in the Measurements of Surfaces and Thin Films*; Passaglia, E., Stromberg, R. R., Kriger, J., Eds.; NBS Publ. No. 256; National Bureau of Standards: Washington, DC, 1964.
(26) Schwartz, D. K.; Steinberg, S.; Israelachvili, J.; Zasadzinski, J. A. *Phys. Rev. Lett.* **1992**, *69*, 3354.
(27) Green, J.-B.; McDermott, M. T.; Porter, M. C.; Siperko, L. M. *J. Phys. Chem.* **1995**, *99*, 10960. Berger, C. E.; van der Werf, K. O.; Kooyman, R. P.; de Grooth, B. G.; Greeve, J. *Langmuir* **1995**, *11*, 4188.
(28) Frisbie, C. D.; Rozsnyai, L. W.; Noy, A.; Wrington, M. S.; Lieber, C. M. *Science* **1994**, *265*, 2071. Noy, A.; Frisbie, C. D.; Rozsnyai, L. F.; Wrighton, M. S.; Lieber, C. M. *J. Am. Chem. Soc.* **1995**, *117*, 7943. Akari, S.; Horn, D.; Keller, H.; Schrepp, W. *Adv. Mater.* **1995**, *7*, 549. Nakagawa, T.; Ogawa, K.; Kurumizawa, T.; Ozaki, S. *Jpn. J. Appl. Phys.* **1993**, *32*, L294. Alley, R. L.; Komvopoulos, K.; Howe, R. T. *J. Appl. Phys.* **1994**, *76*, 5731. Vezenov, D. V.; Noy, A.; Frisbie, C. D.; Rozsnyai, L. F.; Lieber, C. M. *J. Am. Chem. Soc.* **1997**, *119*, 2006. Frommer, J. E. *Thin Solid Films* **1996**, *273*, 112. Noy, A.; Vezenov, D. V.; Lieber, C. M. *Annu. Rev. Mater. Sci.* **1997**, *27*, 381.
(29) Schneider, M.; Frantz, P.; Granick, S. *Langmuir* **1996**, *12*, 994.
(30) Bauer, E. *Z. Kristallogr.* **1958**, *110*, 372.
(31) Israelachvili, J. *Intermolecular and Surface Forces*; Academic Press: San Diego, 1992.
(32) Stipp, S. *Langmuir* **1996**, *12*, 1884.
(33) Halperin, A.; Tirrel, M.; Lodge, T. P. *Adv. Polym. Sci.*, **1992**, *100*, 33.
(34) Ligoure, C.; Leibler, L. *J. Phys.* **1990**, *51*, 1313; Israels, R.; Leermakers, F. A.; Fleer, G. J.; Zhulina, E. B. *Macromolecules* **1994**, *27*, 3249.
(35) Milner, S. T. *Science* **1991**, *251*, 905.
(36) Pefferkorn, E.; Haouam, A.; Varoqui, R. *Macromolecules* **1989**, *22*, 2677. Toprakcioglu, C.; Dai, L.; Ansarifar, M. A.; Stamm, M.; Motschmann, H. *Prog. Colloid Polym. Sci.* **1993**, *91*, 83. O'Shea, S. J.; Welland, M. E.; Rayment, T. *Langmuir* **1993**, *9*, 1826.
(37) Karim, A.; Tsukruk, V. V.; Douglas, J.-F.; Satija, S. K.; Fetters, L. J.; Reneker, D. H.; Foster, M. D. *J. Phys. II*, **1995**, *5*, 1441.
(38) Tsukruk, V. V.; Rinderspacher, F.; Bliznyuk, V. N. *Langmuir* **1997**, *13*, 2171.
(39) Mansfield, M. L. *Polymer* **1996**, *37*, 3835.
(40) Adamson, A. W. *Physical Chemistry of Surfaces*; John Wiley & Sons: New York, 1990.
(41) Linse, P. *Macromolecules* **1996**, *29*, 326.
(42) Tirado, J. D.; Acevedo, D.; Bretz, R. L.; Abrufia, H. D. *Langmuir* **1994**, *10*, 1971.
(43) Offord, D. A.; Griffin, J. H. *Langmuir* **1993**, *9*, 3015.
(44) Nikitas, P. *J. Phys. Chem.* **1996**, *100*, 15247.
(45) Eisenberg, A.; King, M. *Ion Containing Polymers: Properties and Structures*; Academic Press: New York, 1977.
(46) Lipatov, Yu. S. *Colloidal Chemistry of Polymers*; Elsevier: Amsterdam, The Netherlands, 1988.
(47) Lipatov, Yu. S.; Sergeeva, L. *Adsorption of Polymers*; John Wiley: New York, 1974.
(48) Lipatov, Yu. S. *Polymer Reinforcement*; ChemTec Publ.: Toronto, 1995.

MA961897G